

Calibrating density functionals with $DMol^3$ applied on lithium oxide battery

J. H. Pacheco Sánchez, A. Vera García, and L. A. Desales Guzmán

*TecNM / Instituto Tecnológico de Toluca,
Av. Tecnológico s/n. Col. Agrícola Bellavista, Metepec 52149, Edo. Mex., México.*

I.-P. Zaragoza

*TecNM / Instituto Tecnológico de Tlalnepantla,
Av. Mario Colín s/n. Col. La Comunidad, Tlalnepantla de Baz 54070, Edo. Mex., México.*

Received 6 February 2023; accepted 23 August 2024

Density functional theory - based methods constitute part of the computational techniques considered for finding energy, temperature, pressure, density, electronic structure, and more, of materials and other systems. There is not a general density functional for solving either one or another system, rather there are approximations to the exchange-correlation functional designed to apply this theory, and the density functional for the system in study is usually selected through the Jacob's Ladder. The purpose of this article is to calibrate by means of selecting multiple density functionals, for calculating potential energy curves on a specific system, and comparing these results with literature values to determine the most suitable functional. With this theory, when a calculation becomes cyclical means that it does not converge after thousands of steps or iterations. The use of thermal smearing calculations can achieve the convergence of the molecular systems. The density functional is calibrated at insignificant thermal smearing values (around 0.005 Hartrees), because the calculated minimum energy is still consistent against experimental values. This level of theory allows searching for stable reaction products. Among the interactions developed to find a suitable density functional are $\text{Li} + \text{O}$, $\text{Li} + \text{O}_2$, $\text{Li} + \text{CO}$, $2\text{LiO}^- + \text{C}_{38}\text{H}_8$. We select GGA-PBE-Grimme as the most suitable density functional. The resulting information is for applying it to infer about charge/discharge of a rechargeable battery, according to the porosity of the cathode.

Keywords: DFT functionals; potential energy curves; battery ion lithium-oxygen; beta-carbyne.

DOI: <https://doi.org/10.31349/RevMexFis.71.010402>

1. Introduction

The aim of this study is to optimize one way to select a more proper density functional for the studied system in DFT (Density Functional Theory) through calculations of potential energy curves. DFT-based methods are to find potential energy curves by calculating single points step by step among other things. It is known that it does not exist a general functional for solving any different problem. Among the models of density functional designed to apply DFT for the material in study, Jacob's Ladder is a tool for selecting one proper. In this case, with a generalized gradient approximation (GGA) we used BP, VWN-BP, PBE, RPBE, PBE-Grimme, and we also used hybrid GGA with B3LYP, and B3LYP-Grimme. Then, constructing potential energy curves by single point calculations on one system by various density functional for choosing one of them after calibrating each one according to the experimental value. The result is to infer charge/discharge of a rechargeable battery, according to the porosity of the cathode. Furthermore, when a DFT calculation becomes cyclical, there is no convergence after thousands of iterations, however using thermal smearing calculations the convergence of the molecular systems is possible. At thermal smearing values around 0.005 Ha the density functional is calibrated. On this level of theory, we can be able to search stable reaction products.

The thermal smearing computation shows a heating or increase in the temperature of the system, which is not significant when the values are around 0.005 Ha [1], depending on the material used. The latter is based on the change of temperature (T [K]) and pressure (P [atm]) due to thermal smearing variation δE [Ha] at a volume of 638 \AA^3 as shown in Table I of Ref. [2], and a graph corroborating the variation of the energy as a function of the thermal smearing. However, a widely research on this aspect has been carried out in the reference [3] providing reliable convergent results at 0.0001 Ha (0.00272 eV) in cluster calculations $DMol^3$ according to the La and Lu atoms adsorbed on graphene. In the best case, we can achieve a better approximation towards experimental (or theoretical) values when the density functional is calibrated. In the worst case, we can find a density functional that can achieve calculations for the system in study. Here, DFT theory is to search for a stable molecular intermediate of reactions as: $\text{Li} + \text{O}$, $\text{Li} + \text{O}_2$, $\text{Li} + \text{CO}$, $2\text{LiO}^- + \text{C}_{38}\text{H}_8$, which are among those to be developed to obtain information for choosing a functional to infer about the material used in the cathode of a rechargeable battery, because lithium ion is the material of its anode. A rechargeable battery consists of two electrodes (anode and cathode) separated by a membrane. In this case, we propose β -Graphyne as the main material of the cathode.

β -Graphyne is an allotrope of carbon that has diamond-like properties; that is to say, carbons fully bond with other carbons without bonding with another different atom such as hydrogen. There are three known types of graphyne: $\alpha - \beta - \gamma$ -graphyne. Graphyne spreads out like a flat mesh just as graphene does it, but with uniform, non-random porosity. With graphyne, what we intend is to build ordered activated carbon, which has a pore size distribution that can be manipulated, depending on the facilities provided by the graphyne type. It is known that there are batteries or cells with catalytic carbon support, which in the best case is activated carbon with random porosity. Activated carbon has the property of being of high porosity, or a large superficial area, with a dispersion from small to large pores, whereby the pore size distribution is not uniform [4-8].

Research on rechargeable batteries (cells) is still open for industrial applications, such as electric vehicles and electro-mobile devices (cell phones and laptops). The focus is on rechargeable Li-ion batteries, and on electrical energy storage devices which must have high energy density. For this, *metal*-O₂ batteries (Zn-O₂, Al-O₂, Li-O₂) are attractive. These batteries are characterized by having oxygen among their electroactive materials. This simplifies the design and increases the energy density of a battery. For the anode of *metal*-O₂ battery, the metal used can be for example: Ca, Al, Fe, Cd and Zn [9]. Research on Zn-O₂ and Li-O₂ batteries is of interest, and the former is a mature technology. Major part of it, is contemplated in non-rechargeable batteries [9]. Table II in Ref. [10] gives the most common commercial battery systems.

Zinc-oxide Zn-O₂ batteries have a theoretical energy density of 1 kWh/kg, five times above current lithium batteries [11]. Lithium-oxide Li-O₂ or *Li-air* batteries are an alternative with high theoretical gravimetric energy density (11 – 13 kWh/kg). There are four types of cells with respect to the electrolyte used: aprotic, aqueous, solid and hybrid aqueous/aprotic. The efficiency of *Li-air* batteries is lower than 70 %, the low charge and discharge speeds or effect of charge/discharge which is its cyclability, are limitations of this type of battery. Therefore, it is sought to develop materials with better stability, and better efficiency in the reaction and transport kinetics [11]. Li-CO₂ rechargeable batteries with graphene support are designed, identifying the discharge product with first principles calculations [12]. It is concluded that its kinetic parameters must be improved to achieve the efficiency of Li-O₂ batteries [12]. To fabricate and characterize long-cycle Li-O₂ rechargeable cells, a lithium metal anode, a membrane laminate made of glass-ceramic and polymer-ceramic materials, and a solid-state cathode made of air and carbon are needed [13].

The cells (or batteries) are thermally stable with a recharge capacity between 30 and 105°C. A cell achieves 40 discharge/charge cycles. The reproducibility of its design allows the manufacture of safe, rechargeable lithium-air batteries with high energy density [13]. In the development [14] of non-aqueous LiO₂ batteries based on LiOH to avoid instabil-

ity of their typical discharge products: LiO₂ and Li₂O₂. The use of the redox pair I^-/I_3^- is introduced to mediate the oxidation and reduction reactions of LiOH-based, and ionic liquid containing *Li* and water to demonstrate reversible Li-O₂ battery cycle based on LiOH. The addition of the ionic liquid increases the oxidizing power of I_3^- , changing the charging mechanism from the formation of IO/IO_3 to the evolution of O₂ [14].

We build here potential energy curves for several different density functionals used in DFT with the generalized gradient approximation for choosing one, which better approximate to experimental values. We also accomplish some calculations for the interaction between Lithium ion and β -graphyne. From this, we obtained two curves in one graph exhibiting activating and dissociation energies. Our final aim is to get a value for the specific surface area, which can be used to get an average porosity of the material used, which we think it is the main reason for a good efficiency of a battery.

2. Methodology

With the use of Density Functional Theory *DMol*³ [15] from BIOVIA Materials Studio software [16] calculations of minimum energy are carried out. This level of theory is useful to figure out systems properties up to tens of electrons in a spatial dependence of the electron density. *DMol*³ software allows calculations for energy, geometry optimization, dynamics, transition states, elastic constants, reaction kinetics and electron transport. A molecular simulation is useful given its ability as alternative to experimental synthesis [17]. The facilities provided by DFT allow atom-atom, atom-molecule, molecule-molecule interactions to be calculated, of which simple cases are facing a lithium atom and an oxygen atom, a lithium atom and an oxygen molecule, a lithium atom with a molecule of CO, a molecular unit of β -graphyne with an ion of lithium oxide. For example, lithium dioxide can be obtained at least in two ways. One is with the interaction between a lithium atom and an oxygen molecule, and the other is the interaction of a lithium dimer with a carbon dioxide molecule.

DFT [18-21] is employed to perform energy calculations essential for constructing potential energy surfaces that allow observing the adsorption of the two reactants. At thermal smearing values around 0.005 Ha the system encounters a change in temperature, which is slight and insignificant when the values are around 0.005 Ha. It is at these values that a density functional can be calibrated. In this case, this level of theory makes it possible to search for stable reaction products. Geometry optimization calculations allows equilibrium, and consequently stability of a complex intermediate molecule formed between the reactants; in this case, they conduct to the formation of a lithium oxide molecule. Single point step by step calculations can take us to get the interaction between a lithium atom and an oxygen molecule. This is through the construction of potential energy surfaces (curves

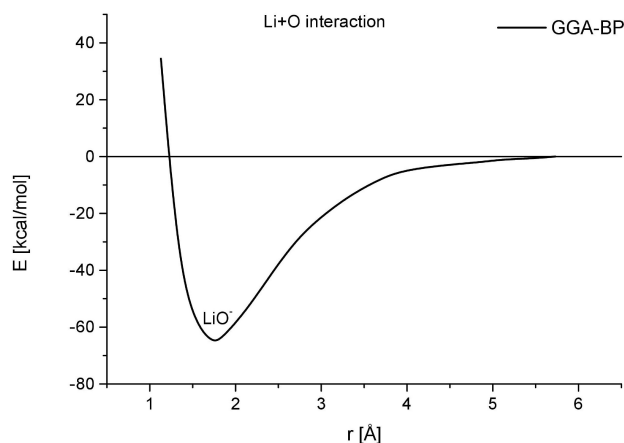


FIGURE 1. Well of potential of *Li*+*O* interaction with equilibrium point at (1.76Å, 66.88 kcal/mol) by means of BP functional.

in our cases), which are also all-electron, *DMol*³ software with DFT-GGA level of theory using a set of DND bases for Hartree-Fock spin unrestricted, and density functional: BP, VWN-BP, PBE, RPBE, PBE-Grimme, B3LYP, and B3LYP Grimme. The same method is used for choosing frequency calculations, which is an additional option for achieving either energy or geometry optimization calculations. When calculations become cyclical without converging, we use thermal smearing to break out the cyclical process, although sometimes a slight bulge appears in the potential wells.

3. Results

First, the interaction between a lithium atom and an oxygen atom is obtained, as it is seen in Fig. 1. Single-point calculations of all-electron interaction between a lithium atom and an oxygen atom are in a level of theory DFT-GGA-BP-UHF carried out with DND 3.5 basis set using 0.003 Ha of thermal smearing, because at 3.73 Å, of separation distance between the two atoms, calculations turn to be cycli-

cal without smearing. This potential energy curve is completed for thermal smearing of 0.003 Ha since 3.7 Å, and shows the formation of a lithium oxide ion LiO^- with a bond that corresponds to chemisorption due to the size of the potential well, which is around 66.88 kcal/mol (see Fig. 1) with length bond of 1.762 Å. The error in the energy calculation is 14.0% with respect to the dissociation energy value of $D_0 = 3.37$ eV (77.8 kcal/mol) for the $X^2\Pi$ state reported by means of *ab initio* CI [22] wave functions calculations, with bond length of 1.695Å, for a reference configuration $1\sigma^2 2\sigma^2 3\sigma^2 4\sigma^2 5\sigma 1\pi^3$ that properly dissociates $\text{Li}:^2\text{S}$ and $\text{O}:^3\text{P}$ [22]. This theoretical computed *ab initio* CI energy is in complete agreement with the experimental value 3.39 ± 0.26 eV [78.175 ± 5.996 kcal/mol] reported on Ref. [23].

The formation of LiO^- with an overestimation greater than 10% when compared against experimental results does not say that it is an appropriate density functional for the calculations. Figure 2 shows a pertinent analysis that allows us an adequate use of thermal smearing to calibrate the chosen density functional whenever possible. In this case, we see that as larger the thermal smearing, the dissociation energy is closer to the experimental value, but the temperature/pressure inadequately grows. Then, for thermal smearing of 0.01 Ha the equilibrium (1.727Å, -70.818 kcal/mol) point has an energy with 9% error respect to that on Ref. [22]. A bond length with error of 1.89% compared against the *ab initio* CI value of Ref. [22] mentioned in the previous paragraph, which is a theoretical result in excellent agreement with the experimental one. It must be noticed that in Fig. 2 normalized means a translational position of the curve in the graph as it is shown in Fig. 2a), which is not applied in Fig. 2b).

However, in all electron calculations using GGA-PBE-GRIMME-UHF with 0.032 Ha of thermal smearing and DND basis set with file 4.4 as seen in Fig. 3, the equilibrium point is obtained at (1.651Å, -73.844 kcal/mol), and has an energy with a 5.32% error.

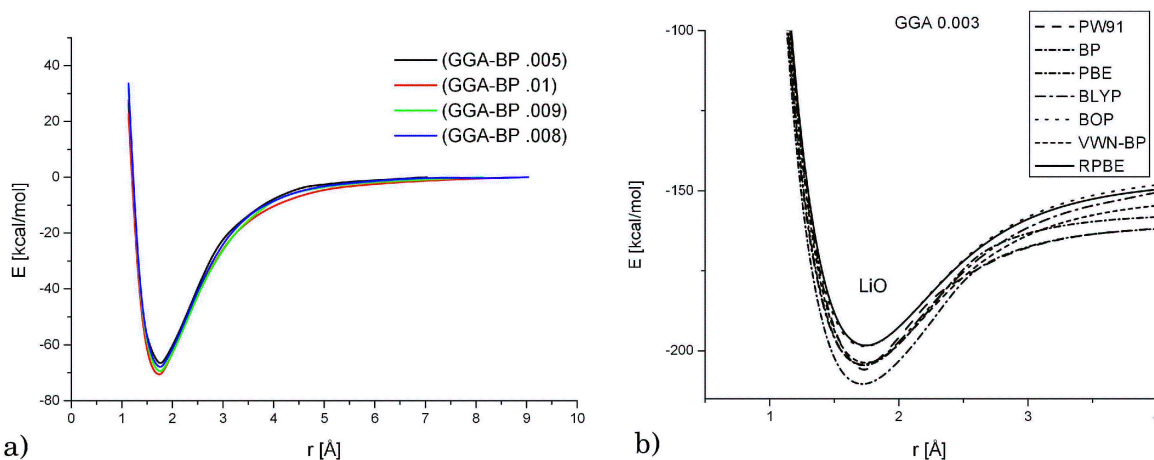


FIGURE 2. Potential energy curves for interaction between lithium and oxygen atoms a) normalized with BP functional at 0.005, 0.01, 0.009, and 0.008 Ha values of thermal smearing, b) without normalizing with PW91, BP, PBE, BLYP, BOP, VWN-BP, RPBE functionals.

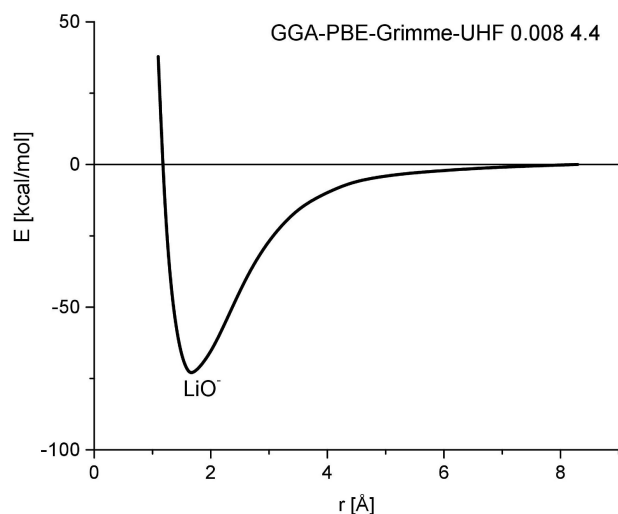


FIGURE 3. Potential energy curve of Li+O interaction using thermal smearing of 0.032 Ha and DND basis set with 4.4 file with PBE-Grimme functional.

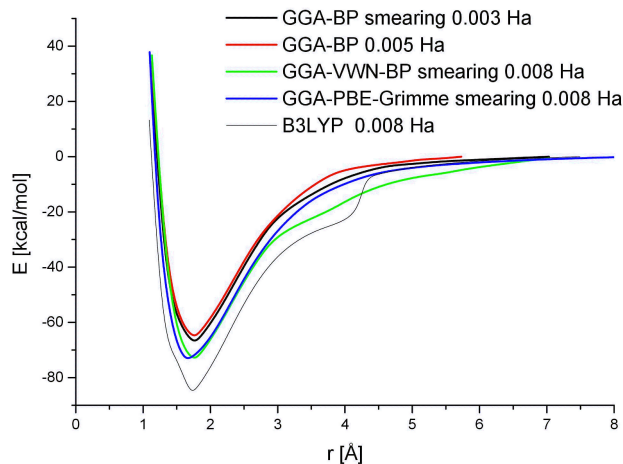


FIGURE 4. Selected functionals BP, VWN-BP and B3LYP to calculate the potential well of the $Li + O$ interaction. The LiO^- formation appears at each different equilibrium points.

The Fig. 4 exhibits a notable enhancement in the approximation to *ab initio* CI results of Ref. [22]. The 5.8% percentage of error in the equilibrium energy point (1.749Å, -73.27 kcal/mol) of GGA-VWN-BP is consequently lower than 10%. In addition, with GGA-PBE-Grimme functional, the calculated energy shows an error of 5.32%, and it is the closest approximation to that one against which we are comparing. Finally, the potential curve of the B3LYP functional exhibits this hybrid functional, with a potential well very irregular, and an equilibrium point (1.722Å, -83.825 kcal/mol) having an error of 7.7% in the energy with respect to the *ab initio* CI value of Ref. [22]. However, since $E_{B3LYP} > E_{EXP}$ there is no consistency in having a potential well below the experimental energy, and it only occurs due to the step that shows the potential energy curve built with B3LYP, which risks the credibility of this density functional.

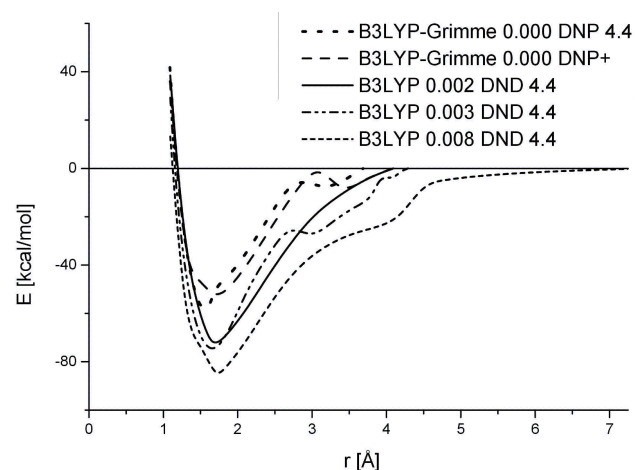


FIGURE 5. Trends of B3LYP functional by using 0.000 Ha, 0.002 Ha, 0.003 Ha, 0.008 Ha values of thermal smearing on Li+O interaction, and DNP, DNP+, DND basis set respectively, the file 4.4.

The case of the B3LYP hybrid functional using DND basis set is explored for the Li+O interaction in Fig. 5. By applying thermal smearing at 0.002 Ha, it is a soft behavior obtained, while it is deforming as its thermal smearing value grows. The curves at 0.002 Ha and 0.003 Ha are similar. About this, at least we must see two things: the first is that as the curve is deforming, the equilibrium point in energy is closer to the experimental value, until it significantly exceeds such value. The second is that the trend to zero is clear when thermal smearing value is 0.032 Ha, while at 0.002 Ha no more points can be by our computational resources obtained. It is inferred that calculating without thermal smearing the minimum of the potential energy curve enhances more, given that the scope in the distance would be lower. These trends show that the use of the B3LYP hybrid functional can be adequate according to the system under study. It is important to mention that each curve has been towards zero normalized by itself that is, using its own value to which the step-by-step procedure in single-point calculations are constant or almost constant according to a tolerance, by taking only one single point taken for all the curves to compare them easily.

From the data for the interactions obtained applying step-by-step single-point calculations, the equilibrium points are in Table I listed.

When directly calculating without thermal smearing in Table I, the results stay far of the experimental values. Sometimes, it is good to calculate thermal smearing at certain value, and then to gradually decrease its value until zero, this gives excellent results; however, in this case we chose to apply calculations directly with the thermal smearing value chosen to see clearly the conduct. Potential energy curves for different density functional at 0.003 Ha of thermal smearing can be observed in Fig. 6a) (notice that once system is stable in the calculations, it is easy to decrease the thermal smearing up to zero with good results), where the minimum energy of GGA-VWN-BP is close to the experimental value 2.55 eV

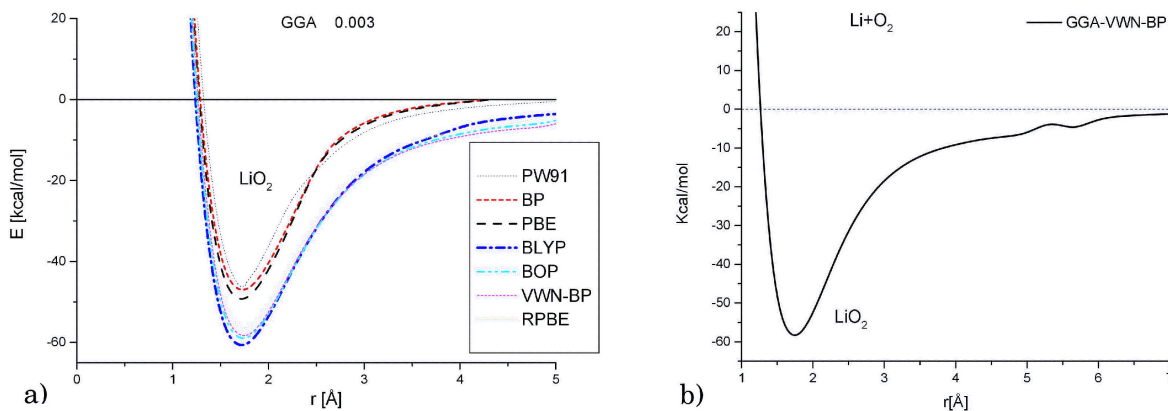


FIGURE 6. Potential energy curves of the interaction between lithium atom and oxygen molecule using the functionals: PW91, BP, PBE, BLYP, BOP, VWN-BP, RPBE. In case of GGA-VWN-BP, the minimum corresponding to the LiO_2 intermediary complex is at the point: a) (1.74Å, -58.32 kcal/mol), b) (1.74Å, -58.53 kcal/mol).

TABLE I. Sensibilizing of equilibrium points [Å, kcal/mol] on Li+O interaction as thermal smearing [Ha] changes for different density functionals.

Functional	Thermal Smearing values [Ha]	Basis set and File	Equilibrium Point [Å, kcal/mol]
UHF GGA-BP	0.000	DND-3.5	(1.730, -65.400)
UHF GGA-BP	0.003	DND-3.5	(1.762, -66.880)
UHF GGA-BP	0.005	DND-3.5	(1.749, -64.810)
UHF GGA-BP	0.032	DND-3.5	(1.709, -70.716)
UHF GGA-BP	0.002	DND-4.4	(1.707, -71.074)
UHF GGA-BP	0.003	DND-4.4	(1.707, -72.325)
UHF GGA-BP	0.005	DND-4.4	(1.705, -71.823)
UHF GGA-BP	0.032	DND-4.4	(1.731, -71.760)
UHF GGA-BP	0.009	DND-4.4	(1.731, -70.282)
UHF GGA-BP	0.010	DND-4.4	(1.695, -68.885)
UHF GGA-VWN-BP	0.003	DND-4.4	(1.706, -72.243)
UHF GGA-VWN-BP	0.005	DND-4.4	(1.731, -69.931)
UHF GGA-VWN-BP	0.032	DND-4.4	(1.699, -73.568)
UHF-GGA-PBE-Grimme	0.032	DND-4.4	(1.697, -73.844)
UHF-GGA-RPBE	0.032	DND	(1.709, -70.716)
B3LYP-Grimme	0.000	DND-4.4	(1.589, -61.696)
B3LYP-Grimme	0.000	DNP+	(1.688, -53.824)
B3LYP	0.002	DND-4.4	(1.693, -72.474)
B3LYP	0.003	DND-4.4	(1.693, -81.764)
B3LYP	0.032	DND-4.4	(1.692, -85.694)

(58.8 kcal/mol) reported on the Ref. [24]; however, GGA-BOP is also very good minimum energy. Here we must comment that in the Ref. [25] the following values were also reported for D_0 dissociation energy Li- O_2 interaction: i) 222 ± 25 kJ/mol (53.06 ± 5.97 kcal/mol) in a flame study measurement by Dougherty *et al.* [26]; ii) 220 kJ/mol (52.58 kcal/mol) semiempirical calculation estimate by Alexander [27]; iii) 302 ± 21 kJ/mol ($72.18 \pm$

5.02 kcal/mol in a flame study measurement by Steinberg and Schofield [28]; iv) ≥ 180 kJ/mol (43.02 kcal/mol) time-resolved kinetics by Plane *et al.* [29]; v) 296 kJ/mol (70.74 kcal/mol) *ab initio* calculation by Plane *et al.*, [29]; vi) 259 kJ/mol (61.9 kcal/mol) *ab initio* calculation by Allen *et al.* [30]. These results indicate a wide diversity in both measurements and theoretical values of D_0 dissociation energy Li- O_2 interaction between lithium (atom) and oxygen

(molecule), then other density functional can approximate another experimental or theoretical value.

In the interaction between a lithium atom and an oxygen molecule $\text{Li}+\text{O}_2$, all electron single-point step-by-step calculations at a level of DFT-GGA-BP theory, the potential energy curve show the formation of a LiO_2 lithium oxide molecule with a bond corresponding to chemisorption due to the magnitude of the well of potential, which is 58.53 kcal/mol (see Fig. 6b) in complete agreement with experimental measurements [24]. The measurement of the dissociation energy of the $\text{Li}-\text{O}_2$ interaction is: 2.55 eV (58.8 kcal/mol) reported by Nefedov *et al.* [24,31], and 2.3 eV (53.06 kcal/mol) reported by Nefedov *et al.*, [24-26].

Nevertheless, in another case in which all electron single-point calculations of the interaction between a lithium atom and an oxygen molecule now at a level of DFT-GGA-BP theory are carried out with a set of DND-3.5 basis set for Hartree-Fock non-restricted spin. In the potential energy curve, the formation of a LiO_2 lithium oxide molecule is observed with bond corresponding to chemisorption due to the magnitude 47.3 kcal/mol of the well of potential (see Fig. 7).

The difference of 5.32% is good result; however, the need to continue searching is due to the diversity of results in this case, and to the existence of frequency calculations for comparing against experimental results. This is a vibrational methodology to investigate a computational result closest to the experimental value. Experimental values of LiO_2 formation in an argon matrix using infrared spectroscopy that correspond to energy levels are next: 492.4 cm^{-1} , 698.8 cm^{-1} , and 1096.9 cm^{-1} [32]. This last value is equivalent to 3.135 kcal/mol ($1\text{ cm}^{-1} = 2,858\text{ cal/mol}$); so, it is not possible to compare against our values calculated through potential energy wells since they are more than 10 times larger, and therefore the comparison is not adequate. This leads to the calculation of frequencies with the same DFT-GGA-BP methodology used, which provides the following frequencies (cm^{-1}) for normal modes: i) 7 : 347.8 , ii) 8 : 658.3 ,

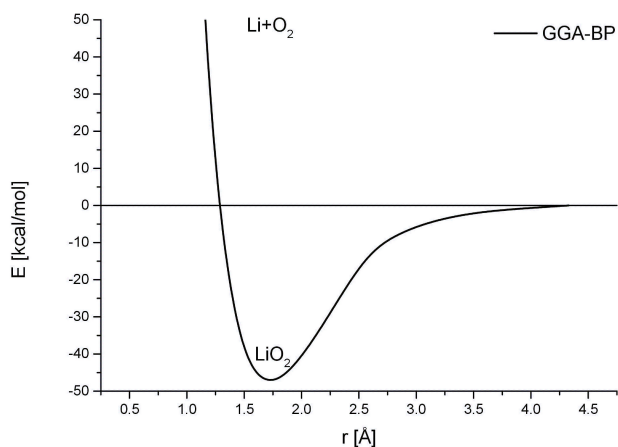


FIGURE 7. Potential energy curve of the interaction between a lithium atom and an oxygen molecule. The minimum at the point (1.7209Å , -47.3265 kcal/mol) corresponds to the LiO_2 intermediary complex by means of BP functional.

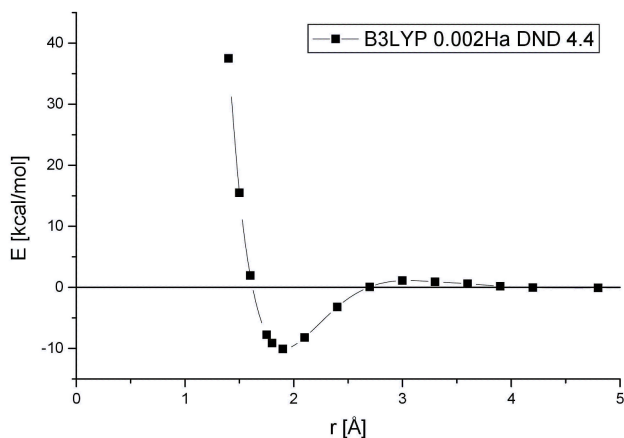


FIGURE 8. Potential energy curve of the $\text{Li}+\text{CO}$ interaction using B3LYP functional with DND basis set file 4.4, at 0.002 Ha of thermal smearing.

iii) 9 : 1670.8 , which are of the same order of magnitude as the experimental values. In addition, the vibrational energy of the zero point is $+3.827\text{ kcal/mol}$ that is 18.07% greater than the experimental, and that reveals an adequate comparison.

The B3LYP hybrid functional has been chosen to calculate the $\text{Li}+\text{CO}$ interaction, and the potential energy curve obtained is in Fig. 8 shown, in which the minimum is located at (1.893Å , -10.53 kcal/mol), and corresponds to the equilibrium point. The distance at this point is the bond length, and the energy is the dissociation energy value, which in this case is far from the experimental value 1806 cm^{-1} (5.1636 kcal/mol) reported in Ref. [33].

In this case, Fig. 9 shows the application of the density functional ones that behaved best in the interactions $\text{Li}+\text{O}$. The eligibility of B3LYP as functional is shown in Fig. 9a), since when comparing it against GGA PBE Grimme, B3LYP gives the best approximation to the experimental value. In Fig. 9b) the calculations are compared without the use of smearing. The minimum of Fig. 9b) when applying the B3LYP hybrid functional is similar to that when thermal smearing 0.002 Ha is used, while by applying GGA-PBE Grimme has the minimum at (2.057Å , -13.423 kcal/mol) with an energy farther to the experimental value than with B3LYP. However, the latter value is in complete agreement with the ab initio result exhibited in reference [34], where the bonding and structure of lithium-ion carbonyl complex Li^+CO was studied at CCSD and MP2 levels of theories, and a global minimum of the Li^+CO complex with bond dissociation energy of 13.7 kcal/mol , and a linear configuration was found.

Finally, the LiO and C_{38}H_8 are molecules independently optimized. The optimized lithium oxide molecule turns out to be the LiO^- ion with hydrogen bond type as shown in Fig. 10a) without visible bond. The C_{38}H_8 molecular unit of carbons ring type β -graphyne [35] alternates single and triple bonds except at four double bonds observed in Fig. 10a) turns out to be flat after geometry optimization.

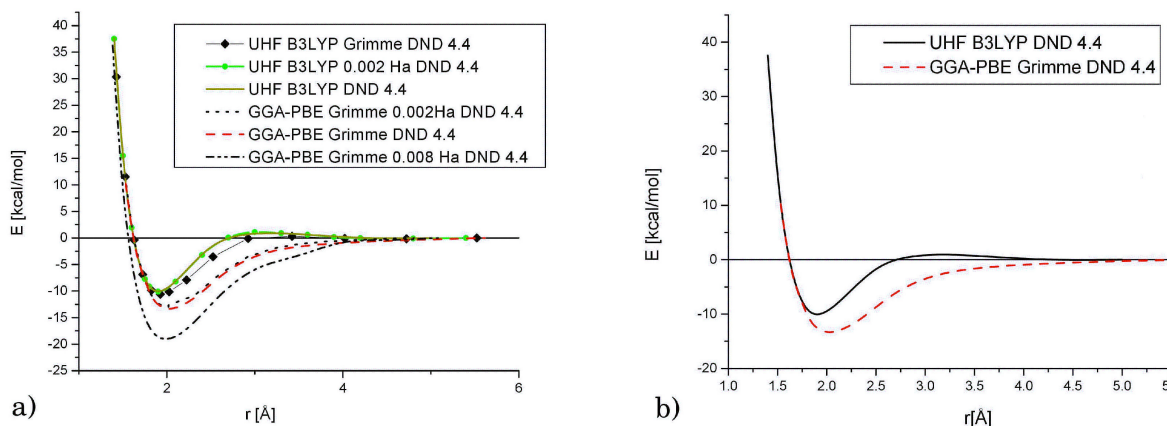


FIGURE 9. a) Comparison among potential energy curves of Li+CO interaction between B3LYP and PBE-Grimme functionals without smearing and at smearing of 0.002 Ha, and 0.008 Ha, b) Specific comparison between B3LYP and PBE-Grimme functionals without smearing.

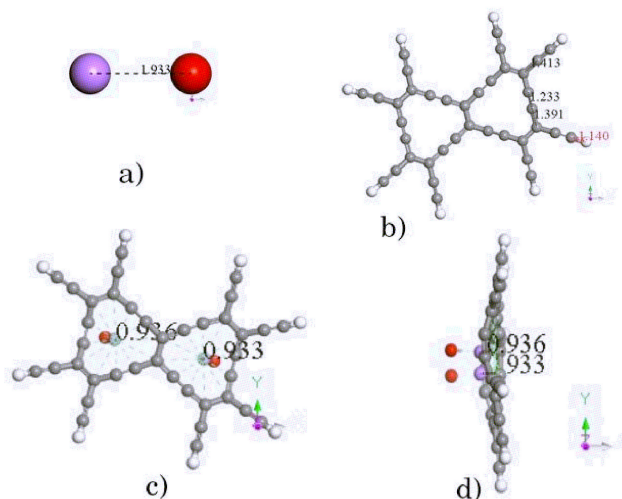


FIGURE 10. Graphyne system with lithium oxide. a) Lithium oxide ion. b) Flat graphyne unit, c) Graphyne unit with two ions of lithium oxide, d) Profile view of the optimized graphyne unit with two lithium oxide ions.

For which DFT-PBE-Grimme-DND-4.4 is used with thermal smearing of 0.007 Ha, with which the resulting energy is -6588.334 kcal/mol (285.605 eV). Each lithium oxide ion is placed approximately in the center of each carbon ring of Fig. 10b). With this configuration we tried about obtaining the potential energy curve that was not possible to obtain. It was only achieved when the complete system was optimized. In this way, choosing the DFT-GGA-PBE-Grimme density functional in all-electron calculations with not restricted spin of Hartree-Fock, with DND basis set using the 4.4 file, without thermal smearing, 'single point' step by step calculations are made about obtaining potential energy curves $2LiO^-$ vs $C_{38}H_8$, placed as seen in Fig. 10c). Figure 10d) shows that after geometry optimization the molecules of lithium oxide make the graphyne unit no longer flat.

In the Fig. 11, we see the potential energy curves of the $2LiO^- + C_{38}H_8$ interaction, where the original energy values were to get energies tending to zero energy translated. Then,

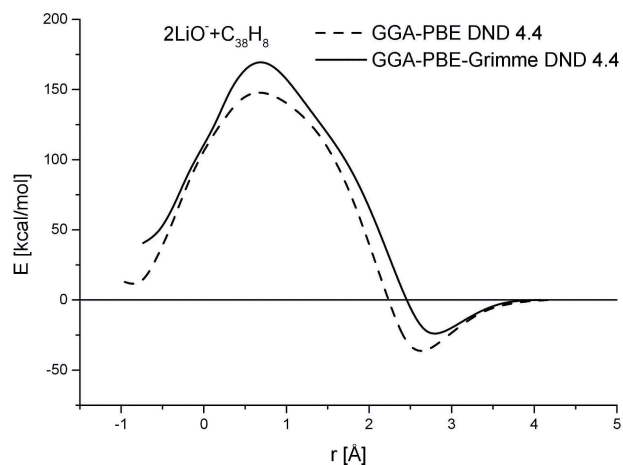


FIGURE 11. Potential energy curves of the $2LiO^- + C_{38}H_8$ interaction. Each curve has two critical points, the PBE curve has maximum at the point (0.658Å, 147.59 kcal/mol), and minimum at (2.64 Å, -35.54 kcal/mol); and the PBE-Grimme curve has maximum at (0.658Å, 168.61 kcal/mol), and minimum at (2.78Å, -24.34 kcal/mol).

maximum and minimum correspond to the energies searched. Each curve has at least two critical points, the PBE curve has a maximum at the point (0.658Å, 147.59 kcal/mol), and a minimum at (2.64Å, -35.54 kcal/mol); and the PBE-Grimme curve has maximum at (0.658Å, 168.61 kcal/mol), and minimum at (2.78Å, -24.34 kcal/mol). The minimums correspond to the formation of an intermediary complex molecule $2LiO^-C_{38}H_8$ for both bond length and dissociation energy.

This lithium oxide ion is a complex case, using another strategy, we were able to get the visible bond between Li and O, and we exhibit in Fig. 12a) such LiO^- ion. Due to the methodology strategy chosen, in this case we proceed to get the adsorption energy using the equation:

$$E_{(ad)} = E_{(LiO-C38)} - E_{(C38)} - E_{(LiO^-)},$$

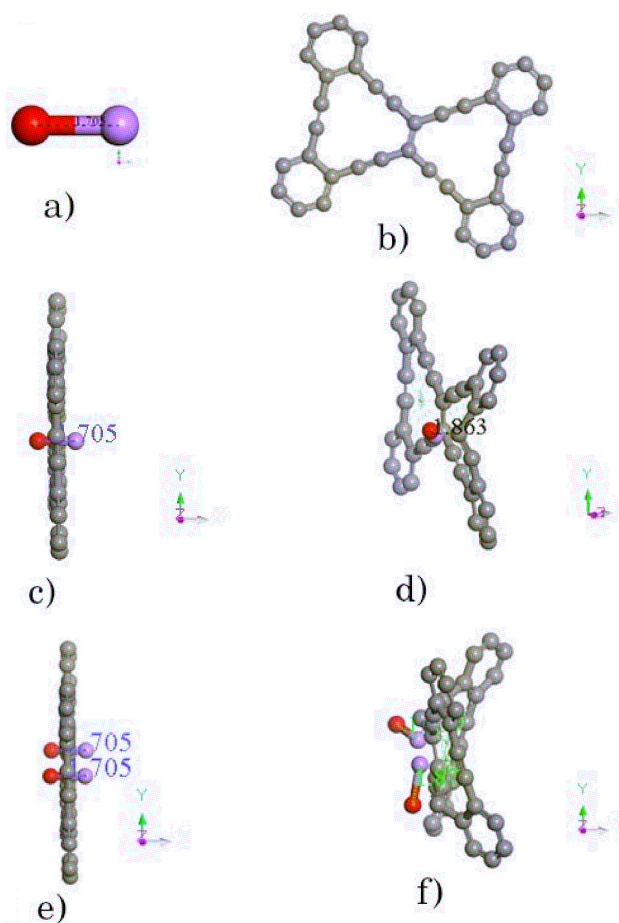


FIGURE 12. β -graphyne system with bonded lithium oxide. a) Lithium oxide ion, b) Flat β -graphyne unit, c) Input for optimization of β -graphyne unit with one ion of lithium oxide, d) Output of the optimized β -graphyne unit with one lithium oxide ion, e) Input for optimization of β -graphyne unit with two ions of lithium oxide, f) Output of the optimized β -graphyne unit with two lithium oxide ions.

where $E_{(\text{LiO}^- \text{C}_{38})} = -6001.020$ kcal/mol is the energy of intermediary complex formed with one lithium oxide ion and one unit of β -graphyne, -92.061 kcal/mol is the energy of one lithium oxide ion, and -5852.783 kcal/mol is the energy of one unit of β -graphyne. Then in this case the adsorption energy of one LiO^- ion and one unit of β -graphyne.

$$E_{(\text{ad})} = -56.354 \text{ kcal/mol.}$$

The adsorption between β -graphyne and lithium-oxide ion is accomplished between one carbon atom attached to β -graphyne and the oxygen atom of Lithium-oxide ion as it is shown in Fig. 12d). Figures 12e) and 12f) exhibit that oxygen is responsible of the planarity deformation of β -graphyne.

Figures 10d), 12d), and 12f) exhibit a charged cathode expecting discharge by the user of the battery.

We achieve one calculation of specific surface area (SSA) [36] on a unit of β -graphyne molecule using the equation

$$A_s = \frac{6}{\rho d},$$

where $\rho = 1.109 \text{ g/cm}^3$ is the density of the material that was with molecular dynamics calculated using the NPT ensemble at 500 ps; and d is an average diameter of a graphyne unit approximately of 13.2 \AA . Then the specific surface area in this case is

$$A_s = 4098.5 \frac{\text{m}^2}{\text{g}}.$$

We consider that this is an excellent specific surface area. On the other hand, using SBET measurements of surface area for activated carbon fiber (ACP) the surface area is $1970 \text{ m}^2/\text{g}$ [37], and our SSA result is 2.32 times greater than this one. We also previously reported activated carbon using burned coconut shells at 900°C a surface area of $452 \text{ m}^2/\text{g}$ using BET measurements [6,38], which is smaller than our result.

4. Discussion

Calculations on $\text{Li}+\text{O}$ have been widely analyzed given that calculations are computationally cheaper than those for the other systems, and we compare our results against data information of diatomic molecules on which we found the dissociation energy near to the experimental value. However, our best results appear by comparing against frequency measurements information for $\text{Li}+\text{O}_2$ and $\text{Li}+\text{CO}$ interactions, for which we selected GGA-PBE-Grimme density functional because the results are the most approximated to either experimental or theoretical results. Our analyses have not been exhaustive, because according to our results, and the systems used, we did not consider obtaining more potential energy curves given that van der Waals interactions supported by PBE-Grimme on gas atoms as oxygen is widely recommended in literature, and results of our calculations agree with this fact. On the other hand, when we perform calculations using thermal smearing values lower than 0.002 the number of iterations grows indicating that it is hard to converge.

On the other hand, ab initio calculations for extended ionic models report that LiO bond of 3.774 au (1.997 \AA) against the experimental value of 3.711 au (1.964 \AA) in their Table I about M-O bond lengths [39]. Ab initio calculations used to provide bond lengths, harmonic frequencies, and dissociation energies of low-lying electronic states for LiO , LiO^+ , LiO^- allowed the electronic structure [40]. There is a close correspondence in the ground states of molecules in which atoms are replaced by other atoms of the same column from the periodic table. An exception to this occurs with the alkali oxides where LiO has a $^2\Pi$ ground state. Ab initio calculations, Hartree-Fock (HF), generalized valence bond (GVB), and configuration interaction (CI) have allowed to elucidate bonding and to explain its reversal [41]. The ground state geometries of neutral and cationic Li_nH ($n = 1 - 7$) and Li_nH_2 ($n = 2 - 6$) clusters are determined in the framework of the SCF and CASSCF procedures. Large-scale CI calculations for valence electrons are to determine stabilities

carried out and ionization potentials (IP) [42]. We are comparing against ab initio CI [22] calculation in agreement with experimental results [23], but another experimental result is $D_0 = 3.49$ eV given at Ref. [43], which is also in agreement with the previous ones.

Using a self-consistent pseudopotential method equilibrium ground-state properties of Mo and Nb transition metals, equilibrium lattice constants, cohesive energies, and bulk moduli, which are in excellent agreement with experiment, have been from calculations obtained [44]. Small nickel clusters were up to the tetramer investigated by the local spin density functional theory. Some competitive states were for the dimer studied. Calculations were by vibrational analysis also followed to discriminate between real minima and saddle points on the potential energy surface. Jahn-Teller deformations played an important role in determining transition-metal cluster geometries. Equilibrium geometries, electronic configurations, binding energies, magnetic moments, and harmonic frequencies were in the work [45] reported. Density-functional theory approach is with fractionally occupied orbitals presented for studying prototypical ferric-ferrous electron-transfer process in liquid water. The use of fractional occupation numbers turned out to be crucial for achieving convergence in most self-consistent calculations because of the open-shell d-multiplet electronic structure of each iron ion and the near degeneracy of the redox groups involved [46].

Density functional theory molecular dynamics (DFT-MD), and classical molecular dynamics using polarizable force fields (PFF-MD) are employed to evaluate the influence of Li^+ on the structure, transport, and electrochemical stability of three potential ionic liquid electrolytes is reported on Ref. [47]. The effect of equilibration methodology and sampling on ab initio molecular dynamics (AIMD) simulations of systems of common solvents and salts found in lithium-oxygen batteries is in Ref. [48] studied.

5. Conclusions

Using Jacob's Ladder, we proposed to work with BP, VWN-BP, PBE, RPBE, PBE-Grimme, B3LYP, and B3LYP Grimme

to construct their potential energy curves for comparing between them, and against experimental values. This brief study lead us to the use of one of the functionals (GGA-BP, GGA-PBE-Grimme, or B3LyP) in the systems required to study lithium oxides with carbon LiO^- support for batteries that improve electric charge storage, ready to be used and discharged by the user of the battery. In this case, it is concluded that GGA-PBE-Grimme gives a minimum with lower energy than GGA-PBE. This is more appreciable for charge desorption in this charge storage system.

The reason to consider LiO^- ion is due to its type $X + Y^-$; that is, an oxidation - reduction process in which one atom loses an electron and the other gain it. Electrons lost on lithium ion is a fact when turns on the device with its corresponding battery, and it must be recharged by external charge by plug in the battery, to which lithium ion recovers its original charge again. This is a reversible process.

Then from the three selected, PBE-Grimme is applied to the interaction between two lithium ions and one β -graphyne unit. Their interaction gives a potential energy curve, from which we see one barrier corresponding to the activation energy, and one well of potential corresponding to the dissociation energy.

We observe that any of the two methodologies (potential energy curves or frequencies) used for choosing the better functional is capable for giving suitable selection. In our case, we selected the construction of potential energy curves in this case. However, the last result of adsorption energy has been with a different method calculated. Furthermore, it is observed that oxygen atom in the lithium oxide ion is responsible for deformation of the planarity of β -graphyne since there is a strong interaction between one carbon atom of β -graphyne and the oxygen atom of lithium oxide ion.

The selected β -graphyne unit molecule has an excellent specific surface area. Then, its use as cathode of Li-ion battery might enhance its capability characteristics.

Acknowledgements

We thank to TecNM for supporting this research through the grant 14113.22-P.

-
1. V.A. Basiuk, Electron smearing in DFT calculations: a case study of doxorubicin interaction with single-walled carbon nanotubes. *Int J Quantum Chem* **111** (2011) 4197-4205.
 2. D. Hernández-Benitez, J. H. Pacheco-Sánchez, Optimization of Chitosan+Activated Carbon Nanocomposite. *DFT Study* **3** (2018) 436, <https://dx.doi.org/10.32474/AOICS.2018.03.000175>.
 3. V. A. Basiuk, O. V. Prezhdo, E. V. Basiuk, Thermal smearing in DFT calculations: How small is really small? A case of La and Lu atoms adsorbed on graphene, *Materials Today Communications* **25** (2020) 101595, <https://dx.doi.org/10.1016/j.mtcomm.2020.101595>.
 4. J. Jagiello, A. Ansón, and M.T. Martínez, *J. Phys. Chem. B* **110** (2006) 4531.
 5. H. Tanahashi, *J. Appl. Electrochem.* **35** (2005) 1067.
 6. L.A. García, I.P. Zaragoza, J.H. Pacheco, A. Bravo, J.L. Contreras, J. Salmones, and G. Arriaga, Study of activated carbons from different source, used to storage hydrogen as energy vector, presented at the 14th International Symposium on Metastable and Nano Materials, Corfu, Greece, 2007.

7. A. Allwar, Bin Md Noor and A. Bin Mohd Nawi, *Journal of Physical Science* **19** (2032) 93.
8. D. Lozano-Castelló, D. Cazorla-Amorós, and A. Linares-Solano, *Energy & Fuels* **16** (2002) 1321.
9. U. Pau. Taylor Peter, Bolton Ronan, Stone Dave, Zhang Xiaoping, Martin Chris, Pathways for Energy Storage in the UK Pathways for energy storage in the UK, (2012).
10. M. Winter, R. J. Brodd, What are batteries, fuel cells, and supercapacitors? *Chem. Rev.* **104** (2004) 4245-4269.
11. M. Gil-Austi, L. Zubizarreta-Saenz De Zaitegui, V. Fuster-Roig, and A. Quijano- López, Batteries of the future: challenges and projection, *Dyna*, **92** (2017) 601-605.
12. Z. Zhang *et al.*, The First Introduction of Graphene to Rechargeable Li - CO₂ Batteries **, *Angewandte Chemie International Edition*, **127** (2015) 6550, <https://dx.doi.org/10.1002/anie.201501214>.
13. B. Kumar *et al.*, A Solid-State, Rechargeable, Long Cycle Life Lithium -Air Battery, *Journal of The Electrochemical Society*, **157** (2010) 50, <https://dx.doi.org/10.1149/1.3256129>.
14. I. Temprano *et al.*, Toward Reversible and Moisture-Tolerant Aprotic Lithium-Air Batteries Toward Reversible and Moisture-Tolerant Aprotic Lithium-Air Batteries, *Joule*, **4** (2020) 2501, <https://dx.doi.org/10.1016/j.joule.2020.09.021>.
15. B. Delley, An all-electron numerical method for solving the local density functional for polyatomic molecules, *J. Chem. Phys.* **92** (1990) 532, <https://dx.doi.org/10.1063/1.458452>.
16. BIOVIA Materials Studio (2017) Springer, New York, USA. (DS BIOVIA. Dassault Systèmes BIOVIA. Retrieved 24 January 2017).
17. D. FairÃ©n-JimÃ©nez, Claves de la simulaci3n molecular para el estudio de procesos de adsorci3n en estructuras metal-orgÃ¡nicas, *An. Quím.* **106** (2010) 183-190.
18. Kohn, W. v-Representability and density functional theory. *Phys. Rev. Lett.* **51** (1983) 1596-1598.
19. Kohn, W. Density-functional theory for excited states in quasi-local density approximation. *Phys. Rev. A.* **34** (1986) 737-741.
20. Kohn, W., and Sham Self-consistent equations including exchange and correlation effects. *Phys. Rev.* **140** (1965) A1133-A1138.
21. Kohn, W. and Vashishta, P. General density functional theory. In *Theory of inhomogeneous Electron Gas.* (Lundqvist, S. and March, NH, eds. Plenum, NY, 1983).
22. M. Yoshimine Accurate potential curves and properties for X 2Π and A 2Σ⁺ states of LiO* *J. Chem. Phys.* **57** (1972) 1132, <https://dx.doi.org/10.1063/1.1678366>.
23. L. Brewer, G. M. Rosenblatt, *Advan. High Temp. Chem.* **2** (1969) 1.
24. A. P. Nefedov, B. V. Rogov, V. A. Sinel'shchikov, and M. A. Khomkin, Investigation of Distribution of Lithium Atoms in the Boundary Layer of the Flow of Combustion *Products High Temperature*, **38** (2000) 742, <https://dx.doi.org/10.1007/BF02755927>.
25. J. M. C. Plane, B. Rajasekhar, and L. Bartolotti, Kinetic study of the reaction potassium + oxygen + M (M = nitrogen, helium) from 250 to 1103 K *J. Phys. Chem.*, **94** (1990) 4161,
26. G. J. Dougherty, M. J. McEwan, L. F. Phillips, Some photometric observations of trace additives in dry carbon monoxide flames *Combust. Flame* **21** 1973 253.
27. M. H. Alexander, Semiempirical potential surfaces and dynamical considerations for collisions between alkali metals and molecular oxygen: Li + O₂ and Na + O₂ a) *J. Chem. Phys.* **69** (1978) 3502, <https://dx.doi.org/10.1063/1.437055>.
28. M. Steinberg, K. Schofield, The High-Temperature Chemistry and Thermodynamics of Alkali Metals (Lithium, Sodium and Potassium) in Oxygen Rich Flames. Preprint; Western Section, The Combustion Institute, November 1987.
29. J. M. C. Plane, B. Rajasekhar, L. Bartolotti, Theoretical and Experimental Determination of the Lithium and Sodium Superoxide Bond Dissociation Energies, *J. Phys. Chem.* **93** (1989) 3141, <https://dx.doi.org/10.1021/j100345a052>.
30. W. D. Allen, D. A. Horner, R. DeKock, R. B. Remington, H. F. Schaefer, The Lithium Superoxide Radical: Symmetry Breaking Phenomena and Potential Energy Surfaces. Submitted for publication in *Chem. Phys.*
31. R.H. Lamoreaux, and D.L. Hildenbrand, High Temperature Vaporization Behavior of Oxides. I. Alkali Metal Binary Oxides. *J. Phys. Chem. Ref Data*, **13** (1984) 151-173.
32. X. Wang, L. Andrews, Infrared spectra, structure and bonding in the LiO₂, LiO₂Li, and Li₂O molecules in solid neon *Molecular Physics: An International Journal at the Interface between Chemistry and Physics*, **107** (2009) 739, <https://dx.doi.org/10.1320/00268973202526583>.
33. O. Ayed, A. Loutellier, L. Manceron, and J. P. Perchard Interaction between Lithium and Carbon Monoxide. 1. A Matrix Infrared Study. *J. Am. Chem. Soc.* **132** (1986) 8138.
34. J. N. Dawoud, Interaction energies and structures of the Li+(CO)_n (n=1-3) complexes. *J. Chem. Sci.* **129** (2017) 543, <https://dx.doi.org/10.1007/s12039-017-1275-5>.
35. X Kim BG, Choi HJ. Graphyne: Hexagonal network of carbon with versatile Dirac cones. *Phys. Rev. B.* **86** (2012) 115435.
36. D.H. Everett, Basic Principles of Colloid Science. Royal Society of Chemistry, (London 1988).
37. IUPAC commission on Colloid and Surface Chemistry Including Catalysis, *Pure Appl. Chem.* **57** (1985) 603.
38. J.H. Pacheco-Sánchez, IP Zaragoza-Rivera, A Bravo-Ortega, Interaction of small carbon molecules and zinc dichloride: DFT study, *Rev. Mex. Fís.*, **63** (2017) 97-110, <https://repositorio.unam.mx/contenidos/4107435>.
39. M. Wilson, Extended ionic models from ab initio calculations, *Phil. Trans. R. Soc. London A* **358** (2000) 399-418.
40. A. I. Boldyrev, J. Simons, Paul von FL Schleyer Ab initio study of the electronic structures of lithium containing diatomic molecules and ions. *The Journal of Chemical Physics* **99** (1993) 8793, <https://dx.doi.org/10.1063/1.465600>.

41. J. N. Allison, R. J. Cave, W. A. Goddard III Alkali Oxides. Analysis of Bonding and Explanation of the Reversal in Ordering of the 2f and 22+States. *J. Phys. Chem.* **88** (1984) 1262, <https://dx.doi.org/10.1021/j150650a049>.
42. V. Bonačić Koutecký, J. Gaus, M.F. Guest, L. Češpiva and J. Koutecký, Ab initio CI study of the electronic structure and geometry of neutral and cationic hydrogenated lithium clusters. Predictions and interpretation of measured properties. *Chem. Phys. Lett.* **206** (1993) 528-539
43. K.P. Huber and G. Herzberg, Molecular Spectra and Molecular Structure **Vol. 4** constants of diatomic molecules. Van Nostrand Reinhold C. NY 1979.
44. C.-L. Fu and K.-M. Ho First-principles calculation of the equilibrium ground-state properties of transition metals: Applications to Nb and Mo. *Phys. Rev. B* **28** (1983) 5480-5486.
45. M. C. Michelini, R. Pis Diez, A. H. Jubert A density functional study of small Nickel clusters. *Inter. J. Quant. Chem.*, **70** (1998) 693-701.
46. A. Migliore, P. H.-L. Sit, and M. L. Klein, Evaluation of Electronic Coupling in Transition-Metal Systems Using DFT: Application to the Hexa-Aquo Ferric-Ferrous Redox Couple. *J. Chem. Theory Comput.* **5** (2009) 307, <https://dx.doi.org/10.1021/ct800340v>.
47. J. B. Haskins, Ch. W. Bauschlicher Jr., and J. W. Lawson, Ab Initio Simulations and Electronic Structure of Lithium-Doped Ionic Liquids: Structure, Transport, and Electrochemical Stability. *J. Phys. Chem. B* **119** (2015) 14705, <https://doi.org/10.1021/acs.jpcc.5b06951>.
48. E. Crabb, A. France-Lanord, G. Leverick, R. Stephens, Y. Shao-Horn, J.C. Grossman* Importance of Equilibration Method and Sampling for Ab Initio Molecular Dynamics Simulations of Solvent-Lithium-Salt Systems in Lithium-Oxygen Batteries. *J. Chem. Theory Comput.* **5** (2009) 307, <https://dx.doi.org/10.1021/acs.jctc.0c03233>.